On the angular dependence of the photoemission time delay in helium

I A Ivanov[1,2], J M Dahlström[3,4,5], E Lindroth[3] and A S Kheifets[1]

[1] Research School of Physics and Engineering, The Australian National University, Canberra ACT 0200, Australia

[2] Center for Relativistic Laser Science, Institute for Basic Science (IBS), Gwangju 500-712, Republic of Korea

[3] Department of Physics, Stockholm University, AlbaNova University Center, SE-10691 Stockholm, Sweden

[4] Max Planck Institute for the Physics of Complex Systems, Noethnitzerstr. 38, 01187 Dresden, Germany

[5] Center for Free-Electron Laser Science, Luruper Chaussee 149, 22761 Hamburg

Abstract.

We investigate an angular dependence of the photoemission time delay in helium measured by the RABBITT (Reconstruction of Attosecond Beating By Interference of Two-photon Transitions) technique. The measured time delay $\tau_a = \tau_W + \tau_{cc}$ contains two distinct components: the Wigner time delay τ_W and the continuum-continuum (CC) correction τ_{cc}. In the case of helium with only one $1s \rightarrow Ep$ photoemission channel, the Wigner time delay τ_W does not depend on the photoelectron detection angle relative to the electric field vector. However, the CC correction τ_{cc} shows a noticeable angular dependence. We illustrate these findings by performing two sets of calculations. In the first set, we solve the time-dependent Schrödinger equation for the helium atom ionized by an attosecond pulse train and probed by an IR pulse. In the second approach, we employ the lowest order perturbation theory which describes absorption of the XUV and IR photons. Both calculations produce close results. These findings are significant as they will guide the next generation of the angular resolved RABBITT experiments which now become feasible.

1. Introduction

The recently developed RABBITT technique (Reconstruction of Attosecond Beating By Interference of Two-photon Transitions) (Muller 2002, Toma and Muller 2002) opened an access to processes taking place on the unprecedentedly short time scale of few tens to few hundreds of attoseconds (1 as = 10^{-18} s). The technique was first employed to measure the duration of attosecond pulses created by high-order harmonic generation (HHG) (Paul *et al* 2001). Then followed a successful application of the RABBITT technique to probe atomic photoionization on its native attosecond time scale. As a first example, the RABBITT technique was used to demonstrated a significant time delay difference between photoemission from the $3s$ and $3p$ shells of argon (Klünder *et al* 2011, Guénot *et al* 2012). In further developments, the relative time delay between the outer shells of the atomic pairs (He vs. Ne and Ne vs. Ar) has been determined owing to active stabilization of the RABBITT spectrometer (Guénot *et al* 2014). Similar measurement has been performed in heavier noble gas atoms relative to the time delay in the $1s$ sub-shell of He (Palatchi *et al* 2014). In conjunction with the HHG, the RABBITT technique has also been used to determine the time delay in Ar (Schoun *et al* 2014).

The RABBITT technique exploits an interference of the two ionization channels leading to the same photoelectron state. It is either absorbing an XUV photon from an odd $2q-1$ harmonic added by absorption of an IR photon ω or ionization by the neighbouring $2q+1$ harmonic followed by emission of the IR photon. Both ionization channels lead to appearance of a side band (SB) in the photoelectron spectrum corresponding to an even $2q$ harmonic. The sideband amplitude oscillates with the relative time delay between the XUV and IR pulses

$$S_{2q}(\tau) = \alpha + \beta \cos(2\omega\tau - \Delta\phi_{2q} - \Delta\theta_{2q}) \tag{1}$$

The delay, τ, denotes a time delay that is used in the RABBITT scheme to delay the IR probe relative to the XUV pump. The term $\Delta\phi_{2q}$ denotes the phase difference between the two neighbouring odd harmonics $2q \pm 1$ which can be converted to the group delay of the attosecond pulse as $\tau_{2q}^{(GD)} = \Delta\phi_{2q}/2\omega$. The quantity $\tau - \tau_{2q}^{(GD)}$ is the delay between the maxima of the IR electric field oscillation and the arrival of the XUV pulse. The additional term $\Delta\theta_{2q}$ arises from the phase difference of the atomic ionization amplitude corresponding to the XUV energies different by 2ω. This phase difference can be converted to the atomic delay $\tau_a = \Delta\theta_{2q}/2\omega$. Thus defined quantity can be represented theoretically as the sum of the two distinct components $\tau_a = \tau_W + \tau_{cc}$ (Dahlström *et al* 2013). Here τ_W is the Wigner-like time delay associated with the XUV absorption and τ_{cc} is a correction due to the IR photon absorption via the continuum-continuum (CC) transition.

The attosecond streak-camera method (Itatani *et al* 2002) is in many regards similar to the RABBITT method, the main difference being that 'streaking' relies on isolated attosecond pulses corresponding to a continuum of XUV frequencies rather than the discrete odd high-harmonics of the RABBITT method (Dahlström, Huillier and Maquet

2012, Pazourek *et al* 2013). The target electron is first ejected by the isolated XUV pulse and it is then streaked: accelerated or decelerated by the IR dressing field. In this technique, the photoelectron is detected in the direction of the joint polarization axis of the XUV and IR fields. So a possible dependence of the atomic time delay on the photoelectron direction is not detected in this technique. The RABBITT measurement is very different in this respect because the photoelectrons are collected from all directions. Hence a possible angular dependence of the time delay may become an issue. Because of the known propensity rule (Fano 1985), the XUV photoionization transition $n_i l_i \rightarrow El$ is dominated by a single channel $l = l_i+1$. In this case, the Wigner time delay is simply the energy derivative of the elastic scattering phase in this dominant channel $\tau_W = d\delta_l/dE$. However, if the nominally stronger channel goes through a Cooper minimum, the weaker channel with $l = l_i - 1$ becomes competitive. The interplay of these two photoionization channels leads to a strong angular dependence of the Wigner time delay because these channels are underpinned by different spherical harmonics. The hint of this dependence was indeed observed in a joint experimental and theoretical study (Palatchi *et al* 2014) near the Cooper minimum in the $3p$ photoionization of argon. This effect was seen as a much better agreement of the angular averaged atomic calculations in comparison with angular specific calculations. That is why the measured Wigner time delay in this experiment was termed an effective time delay. In subsequent theoretical studies, this effect was investigated with more details and an explicit angular dependence was graphically depicted (Wätzel *et al* 2014, Dahlström and Lindroth 2014).

In the case of a single atomic photoionization channel, like $1s \rightarrow Ep$ channel in He, the interchannel competition is absent and the Wigner time delay is angular independent. The early investigations of the τ_{cc} correction (Dahlström, Guénot, Klünder, Gisselbrecht, Mauritsson, Huillier, Maquet and Taïeb 2012) showed no angular dependence of this component on the time delay either. Hence one may think that the RABBITT measured time delay in He should be angular independent. This assumption was challenged in a recent experiment by Keller (2014) and her group in which the RABBITT technique was supplemented with the COLTRIMS (Cold Target Recoil Ion Momentum Spectroscopy) apparatus. This combination made it possible to relate the time delay to a specific photoelectron detection angle relative to the polarization axis of light. The findings of Keller (2014) is significant because the helium atom is often used as a convenience reference to determine the time delay in other target atoms. If the RABBITT measurement is not angular resolved, like in the experiment by Palatchi *et al* (2014), the angular dependence of the time delay in the reference atom may compromise the accuracy of the time delay determination in other target atoms.

This consideration motivated us to investigate theoretically the angular effects in the time delay of helium measured by the RABBITT technique. We perform our investigation by combining the two completely independent approaches. In the first approach, we solve the time-dependent Schrödinger equation (TDSE) which describes the evolution of the helium atom driven by an attosecond pulse train (APT) and an IR dressing field with the single-active electron approximation. After the field is switched

off, we project the solution of the TDSE on the field-free Coulomb states and get the photoelectron spectrum in various directions. We repeat this calculation for various time delays τ between the APT and IR fields and fit the SB intensity oscillations with Equation (1). Because the group delay of the harmonics is known in our calculation, we can extract the atomic time delay and determine its angular dependence for each specific side band. In the second approach, we apply the lowest order perturbation theory (LOPT) which describes the two-photon XUV and IR ionization. Although this method may be less accurate then a non-perturbative TDSE approach concerning the interaction with more substantial field intensities, it is physically very transparent, much less time consuming and while including many-electron screening effects of the XUV photon it allows for inclusion of correlation corrections by infinite-order many-body perturbation theory. The angular dependence of the time delay can be easily interpreted in the LOPT as a competition of the CC transitions $Ep \to E'd$ and $Ep \to E's$ driven the the IR absorption. This competition may become particularly intense near the geometric node of the d-spherical wave at the magic angle $\theta_m = \mathrm{acos}(1/\sqrt{3}) = 54.7°$.

We compare results of these two calculations and draw conclusions.

2. Theory and numerical implementation

2.1. LOPT approach

The RABBITT process can be described using perturbation theory with respect to the interaction with the XUV and IR fields. The dominant lowest-order contributions are given by two-photon matrix elements from the initial electron state i to the final state f by absorption of one XUV photon, ω_x, followed by exchange of one IR photon, ω,

$$M(f,\omega,\omega_x,i) = \frac{1}{i}E(\omega)E(\omega_x)\lim_{\varepsilon\to 0^+}\sum\!\!\!\!\!\!\int_p \frac{\langle\, f \mid z \mid p\,\rangle\langle\, p \mid z \mid i\,\rangle}{\epsilon_i + \omega_x - \epsilon_p + i\varepsilon}, \tag{2}$$

where both fields are linearly polarized along the $\boldsymbol{n}_z$-axis. The single-electron states are expressed as partial wave states $\langle\, \boldsymbol{r} \mid i\,\rangle = R_{n_i,\ell_i}(r)Y_{\ell_i,m_i}(\boldsymbol{n}_{\boldsymbol{r}})$ and $\langle\, \boldsymbol{r} \mid f\,\rangle = R_{k_f,\ell_f}(r)Y_{\ell_f,m_f}(\boldsymbol{n}_{\boldsymbol{r}})$ for bound initial state and continuum final state with corresponding single-particle energies ϵ_i and ϵ_f, respectively. Energy conservation of the process is given by $\epsilon_f - \epsilon_i = \omega_x \pm \omega$, where $+(-)$ corresponds to absorption (emission) of an IR photon. All intermediate unoccupied states, $\langle\, \boldsymbol{r} \mid p\,\rangle = R_{n_p,\ell_p}(r)Y_{\ell_p,m_p}(\boldsymbol{n}_{\boldsymbol{r}})$, are included in the integral sum in Eq.(2). Angular momentum conservation laws applied to the $1s^2$ ground state in helium require that $\ell_i = 0$, $\ell_p = 1$ and $\ell_f = 0, 2$ and $m_i = m_p = m_f = 0$. The two-photon matrix element in Eq. (2) can be re-cast as a one-photon matrix element between the final state and an uncorrelated perturbed wave function (PWF)

$$M(q,\omega,\omega_x,a) = \frac{1}{i}E(\omega_x)E(\omega)\langle\, f \mid z \mid \rho^{(0)}_{\omega_x,i}\,\rangle. \tag{3}$$

The PWF is a complex function that describes the outgoing photoelectron wave packet, with momentum k' corresponding to the on-shell energy $\epsilon' = \epsilon_i + \omega_x$, after absorption of one XUV photon creating a hole in the atomic state i (Aymar and Crance 1980, Toma

and Muller 2002, Dahlström *et al* 2013). Correlation effects due to the screening by other electrons can be systematically included by substitution of the uncorrelated PWF with the correlated PWF based on the Random-Phase Approximation with Exchange (RPAE): $\mid \rho^{(0)}_{\omega_x,a} \rangle \rightarrow \mid \rho^{(RPAE)}_{\omega_x,a} \rangle$. Details about the implementation of such correlation corrections were recently given in Ref. (Dahlström and Lindroth 2014).

Using Eq. (2) and Eq. (14) we construct the complex amplitude for absorption of two photons $\omega_x = (2q-1)\omega$ and ω

$$\mathcal{M}^{(\mathrm{abs})}_{\boldsymbol{k_f}} = (8\pi)^{3/2} \sum_{l_f=0,2} i^{-l_f} e^{i\delta_f} Y_{l_f,0}(\boldsymbol{n_f}) M(f,\omega,\omega_x,i) \tag{4}$$

and for absorption of one photon $\omega_x = (2q+1)\omega$ followed by emission of ω

$$\mathcal{M}^{(\mathrm{emi})}_{\boldsymbol{k_f}} = (8\pi)^{3/2} \sum_{l_f=0,2} i^{-l_f} e^{i\delta_f} Y_{l_f,0}(\boldsymbol{n_f}) M(f,-\omega,\omega_x,i) \tag{5}$$

both leading to the same final state with photoelectron momentum, $\boldsymbol{k_f} = k_f \boldsymbol{n_f}$ with $k_f = \sqrt{2\epsilon_f} = \sqrt{2(2q\omega + \epsilon_i)}$. The probability for directed photoemission is proportional to

$$S_{2q}(\boldsymbol{k_f}) = 2 \left| \mathcal{M}^{(\mathrm{emi})}_{\boldsymbol{k}_f} \exp[i(\phi_{2q+1} - \varphi)] + \mathcal{M}^{(\mathrm{abs})}_{\boldsymbol{k}_f} \exp[i(\phi_{2q-1} + \varphi)] \right|^2 , \tag{6}$$

where we write explicitly the phases of the fields: $\varphi = \omega\tau$ of the ω field and ϕ_{2q+1} and ϕ_{2q-1} of the $\omega_{x\,2q+1}$ and $\omega_{x\,2q-1}$ fields so that the field amplitudes, E, inside $\mathcal{M}$ (and M) are real. The different signs of φ in the terms on the right side of Eq.(6) arise due to the IR photon being either absorbed of emitted in the process, $E(\omega) = |E(\omega)|e^{i\varphi} = E^*(-\omega)$. In connection with Eq. (1) we then obtain the angle-resolved atomic delay

$$\tau_a(\boldsymbol{k_f}) = \Delta\theta_{2q}(\boldsymbol{k_f})/2\omega = \arg[\mathcal{M}^{(\mathrm{emi})}_{\boldsymbol{k_f}} \mathcal{M}^{*(\mathrm{abs})}_{\boldsymbol{k_f}}]/2\omega. \tag{7}$$

2.2. TDSE approach

We solve the TDSE for a helium atom described in a single active electron approximation:

$$i\partial\Psi(\boldsymbol{r})/\partial t = \left[\hat{H}_{\mathrm{atom}} + \hat{H}_{\mathrm{int}}(t)\right] \Psi(\boldsymbol{r}) \ , \tag{8}$$

where $\hat{H}_{\mathrm{atom}}$ is the Hamiltonian of the field-free atom with an effective one-electron potential (Sarsa *et al* 2004). The Hamiltonian $\hat{H}_{\mathrm{int}}(t)$ describes the interaction with the external field and is written in the velocity gauge:

$$\hat{H}_{\mathrm{int}}(t) = \boldsymbol{A}(t) \cdot \hat{\boldsymbol{p}} \quad , \quad \boldsymbol{A}(t) = -\int_0^t \boldsymbol{E}(t')\ dt' \tag{9}$$

As compared to the alternative length gauge, this form of the interaction has a numerical advantage of a faster convergence.

The electric field in the IR pulse is modeled as

$$\boldsymbol{E}_{\mathrm{IR}}(t) = \hat{\boldsymbol{z}}\ E_0\ f(t) \cos\omega t \tag{10}$$

with the envelope function

$$f_{\rm IR}(t) = \begin{cases} 3(t/T)^2 - 2(t/T)^3 & t < T \\ 1 & T < t < (N-1)T \qquad N = 25 \\ 3[(NT-t)/T]^2 - 2[(NT-t)/T]^3 & (N-1)T < t < NT \end{cases} \tag{11}$$

Here $T = 2\pi/\omega \simeq 2.67$ fs with $\omega = 1.55$ eV being the IR frequency. The electric field in the APT is modelled according to Lee *et al* (2012):

$$\boldsymbol{E}_{\rm APT}(t) = \hat{\boldsymbol{z}}\ E_0 \sum_{\xi=-15}^{15} (-1)^\xi \sin[\omega_x(t' - \xi T/2)] \tag{12}$$
$$\times \exp\left[-2\ln 2 \left(\frac{t' - \xi T/2}{\tau_x}\right)^2\right] \exp\left[-2\ln 2 \left(\frac{t'}{\tau_T}\right)^2\right] \quad , \quad t' = t - \Delta\ .$$

The constants $\tau_x = 0.3$ fs and $\tau_T = 25$ fs determine the length of an XUV pulse and the APT train, respectively. The APT is shifted relative to the IR pulse by a variable delay $\Delta \in [12T : 13T]$. An increasing delay $\Delta > 0$ corresponds to the APT moving away from the beginning of the IR pulse towards its end. The amplitudes of the IR and XUV fields were 0.002928 a.u. and 0.000119 a.u. respectively, which corresponds to the field intensity of 3×10^{11} W/cm^2 for the IR and 5×10^8 W/cm^2 for the XUV field.

The APT (12) is visualized in Figure 1 (left) along with its spectral content (right) for the the XUV frequency $\omega_x = 32.5$ eV chosen to match the 21st harmonic.

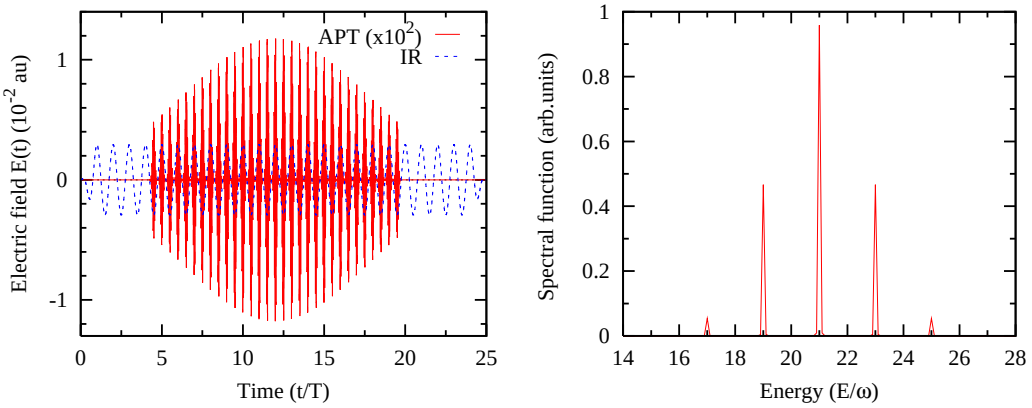

Figure 1. (Color online) The electric field in the APT (red solid line) and the IR pulse (blue dashed line). The XUV frequency $\omega_x = 32.5$ eV in Equation (12) is chosen to match the 21st harmonic. The APT/IR delay $\Delta = 12T$.

To solve the TDSE, we follow the strategy tested in our previous works (Ivanov 2011, Ivanov and Kheifets 2013). The solution of the TDSE is presented as a partial wave series

$$\Psi(\boldsymbol{r}, t) = \sum_{l=0}^{L_{\rm max}} f_l(r, t) Y_{l0}(\theta, \phi) \tag{13}$$

with only zero momentum projections retained for the linearly polarized light. The radial part of the TDSE is discretized on the grid with the stepsize $\delta r = 0.05$ a.u. in

a box of the size $R_{\max} = 400$ a.u. The number of partial waves in Equation (13) was limited to $L_{\max} = 4$ which ensured convergence in the velocity gauge calculations.

Substitution of the expansion (13) into the TDSE gives a system of coupled equations for the radial functions $f_{l\mu}(r,t)$, describing evolution of the system in time. To solve this system, we use the matrix iteration method Nurhuda and Faisal (1999). The ionization amplitudes $a(\boldsymbol{k})$ are obtained by projecting the solution of the TDSE at the end of the laser pulse on the set of the ingoing scattering states of the target atom,

$$\psi_{\boldsymbol{k}}^{(-)}(\boldsymbol{r}) \propto \sum_{l=0}^{L_{\max}} i^l e^{-i\delta_l} Y_{l\mu}^*(\hat{\boldsymbol{k}}) Y_{l\mu}(\hat{\boldsymbol{r}}) R_{kl}(r) \ . \tag{14}$$

Squaring of the amplitudes $a(\boldsymbol{k})$ gives the photoelectron spectrum in a given direction $\hat{\boldsymbol{k}}$ determined by the azimuthal angle θ_k. An example of such spectra in the $\hat{\boldsymbol{z}}$ direction $\theta_k = 0$ and $\theta_k = 60^\circ$ is shown in Figure 2

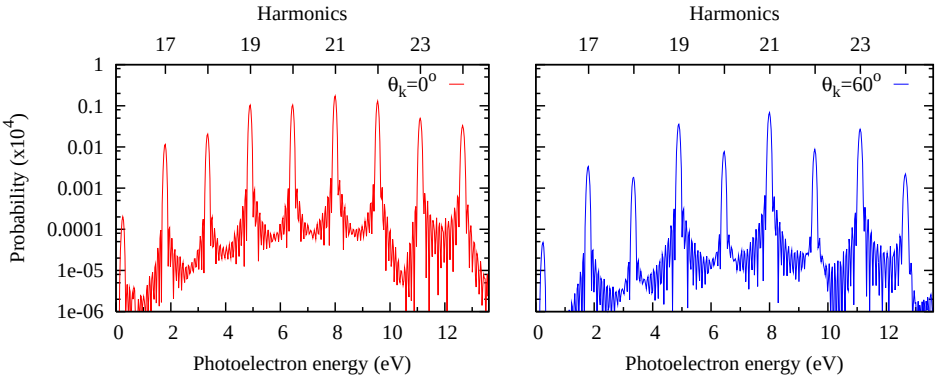

Figure 2. (Color online) The photoelectron spectra detected at the angles $\theta_k = 0^\circ$ (left) and $\theta_k = 60^\circ$ (right)

After collecting the photoelectron spectra in various directions, the SB intensity oscillation with the variable time delay between the APT and IR fields is fitted with the cosine function $A + B\cos[2\omega(\Delta - 3T) + C]$ using the non-linear Marquardt-Levenberg algorithm. The quality of the fit is very good with the errors in all three parameters not exceeding 1%. Several examples of the fit for the SB20 at the photoelectron detection angles $\theta_k = 0^\circ$, 60° and 90° are shown in Figure 3.

The angular dependence of parameters A, B and C for the SB20 is shown in Figure 4. To highlight the partial wave composition of the sideband signal, we plot on the left panel of Figure 4 the squared spherical harmonic $|Y_{20}(\hat{\boldsymbol{k}})|^2 \propto |P_2(\cos\theta_k)|^2$. We see that for small angles $\theta_k < 30^\circ$, this component reflects the angular dependence of the SB amplitude rather well but then, when approaching the "magic angle", there is a noticeable deflection of the SB intensity which means that there is a strong competition between the s- and d-waves and hence an angular dependence of the time delay. We also note that the sideband intensity vanishes at $\theta_k = 90^\circ$ due to destructive interference of the $s-$ and $d-$partial waves.

The corresponding data from the LOPT calculation are shown in the same figure. The LOPT A-parameter is normalized to the same parameter in the TDSE calculation.

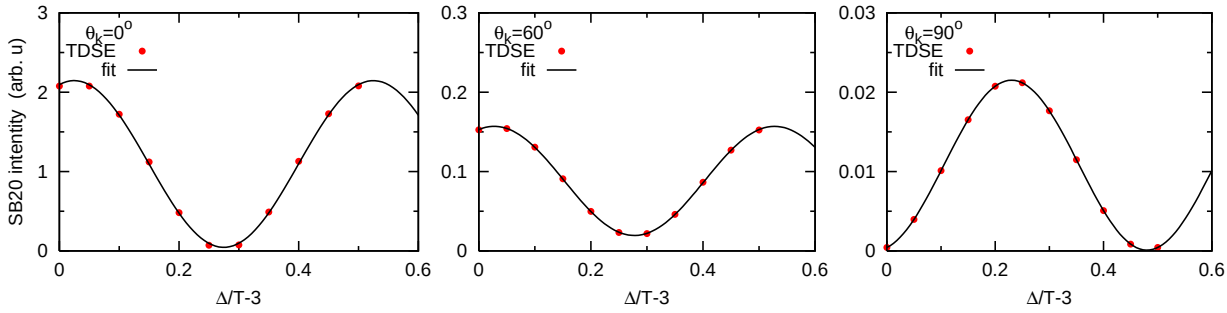

Figure 3. (Color online) The SB20 intensity oscillation as a function of the time delay $\Delta/T - 3$ for the photoelectron detection angles $\theta_k = 0°$, $60°$ and $90°$

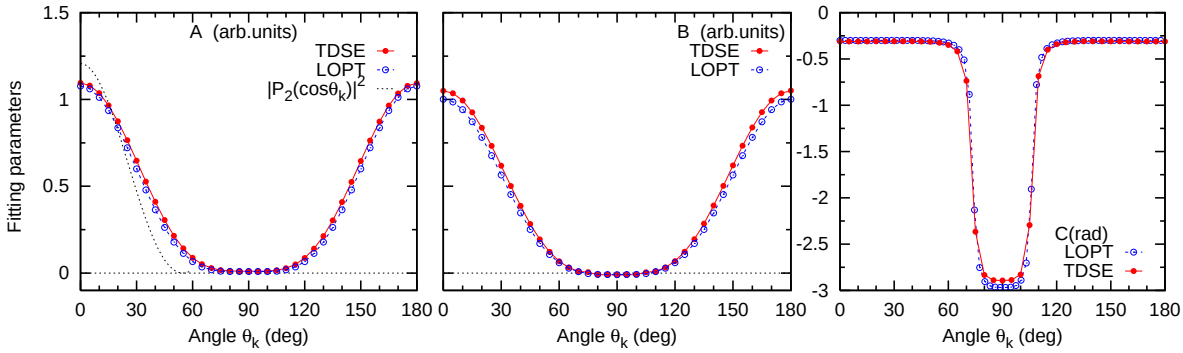

Figure 4. (Color online) Angular dependence of the fitting parameters A, B, and C for the SB20. The TDSE and LOPT calculations are shown with the solid (red) line and dashed (blue) line, respectively. The LOPT calculation is normalized to the TDSE in the maximum of the A parameter. The insets show the variation of the A and B parameters near $90°$.

The same cross-normalization is retained for the B-parameter. The C parameter is plotted on the absolute scale. All the three parameters agree very well between the TDSE and LOPT calculations.

The group delay of the ATP is zero in our model since all the harmonics have the same phase of $\pi/2$ at their spectral maxima. Hence the parameter C can be converted directly into the atomic time delay as $\tau_a = C/2\omega$ according to Equation (1). Thus obtained atomic time delay in the zero direction is given in Table 1 where we show the atomic time delay τ_a in both calculations and its breakdown into the Wigner time delay τ_W and the CC correction τ_{cc}. Again the agreement between the two calculations is excellent.

3. Discussion

Within the 0 to 40° range, where the RABBITT signal is largest, the angular variation of the time delay is rather small, typically of several attoseconds. In the experimentally accessible range up to 60°, only the SB18 displays a noticeable angular dependence of the time delay. Larger angular variation of time delay is observed for larger detection angles

	E	τ_a (as)		τ_W (as)	τ_{cc} (as)	
SB	eV	TDSE	LOPT	RPAE	[1]	[2]
18	3.3	-92	-93	231	-324	-315
20	6.4	-66	-63	60	-123	-129
22	9.5	-50	-48	30	-78	-83

Table 1. Atomic time delay τ_a and its various components τ_W and τ_{cc} in the $\hat{z}$ direction for various side bands.

[1] Atomic delay minus Wigner delay

[2] Fit to exact hydrogen calculation by Richard Taïeb (Dahlström, Guénot, Klünder, Gisselbrecht, Mauritsson, Huillier, Maquet and Taïeb 2012)

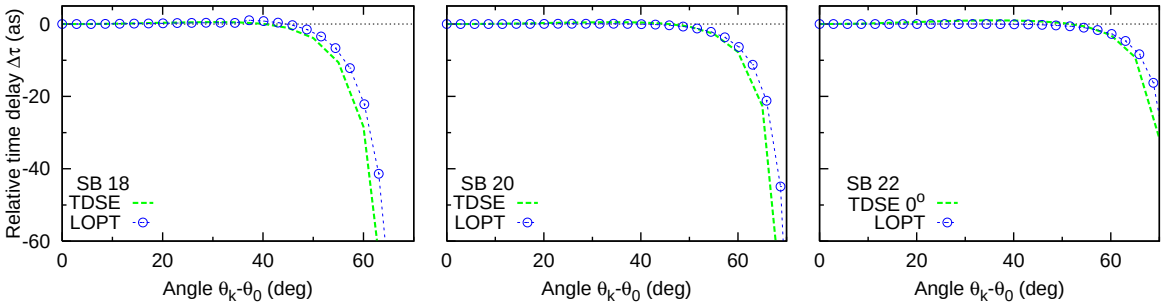

Figure 5. (Color online) Variation of the time delay relative to the fixed angle $\Delta\tau_a = \tau_a(\theta_k) - \tau_a(\theta_0)$ for the SB18 (left), SB 20 (center) and SB22 (right). The TDSE results are shown with the dashed green line. The LOPT calculations shown with the blue open circles.

where the intensity is falling off exponentially. Because the largest angular variation of the time delay falls into the region of small SB intensity, it plays very little role in angular averaged RABBITT experiments. Hence the helium atom can be safely used as the reference atom.

The present non-perturbative TDSE calculation agrees very well the LOPT calculation. An analogous TDSE calculation performed at $I_{APT} = 5 \times 10^8 W/cm^2$ and $I_{APT} = 5 \times 10^8 W/cm^2$ returned very similar results (Alvaro Jiminez Galán and Luca Argenti 2014). This indicates that the XUV field intensity of the order of several units of 10^8 W/cm^2 is still in the linear perturbative regime. Hence the measured time delay should not depend on the exact value of the field intensity. Because the pulse parameters are noticeably different between the present calculation and that of Alvaro Jiminez Galán and Luca Argenti (2014), we expect that their influence on the measured time delay is insignificant.

Acknowledgments

The authors are grateful to Luca Argenti, Ursula Keller, Sebastian Heuser and Claudio Cirelli for many stimulating discussion. JMD acknowledges support from the Swedish Research Council (VR). IA and ASK acknowledge support by the Australian Research Council in the form of the Discovery grant DP120101805. IA acnowledges support from the Institute for Basic Science, Gwangju, Republic of Korea.

References

Alvaro Jiminez Galán and Luca Argenti 2014. private communication

Aymar M and Crance M 1980 Two-photon ionisation of atomic hydrogen in the presence of one-photon ionisation *Journal of Physics B: Atomic and Molecular Physics* **13**(9), L287

Dahlström J, Guénot D, Klünder K, Gisselbrecht M, Mauritsson J, Huillier A L, Maquet A and Taïeb R 2012 Theory of attosecond delays in laser-assisted photoionization *Chem. Phys.* **414**, 53–64

Dahlström J M, Guénot D, Klünder K, Gisselbrecht M, Mauritsson J, L.Huillier A, Maquet A and Taïeb R 2013 Theory of attosecond delays in laser-assisted photoionization *Chem. Phys.* **414**, 53 – 64

Dahlström J M and Lindroth E 2014 Study of attosecond delays using perturbation diagrams and exterior complex scaling *J. Phys. B* **47**(12), 124012

Dahlström J M, Huillier A L and Maquet A 2012 Introduction to attosecond delays in photoionization *J. Phys. B* **45**(18), 183001

Fano U 1985 Propensity rules: An analytical approach *Phys. Rev. A* **32**, 617–618

Guénot D, Klünder K, Arnold C L, Kroon D, Dahlström J M, Miranda M, Fordell T, Gisselbrecht M, Johnsson P, Mauritsson J, Lindroth E, Maquet A, Taïeb R, L'Huillier A and Kheifets A S 2012 Photoemission-time-delay measurements and calculations close to the 3*s*-ionization-cross-section minimum in Ar *Phys. Rev. A* **85**, 053424

Guénot D, Kroon D, Balogh E, Larsen E W, Kotur M, Miranda M, Fordell T, Johnsson P, Mauritsson J, Gisselbrecht M, Varjù K, Arnold C L, Carette T, Kheifets A S, Lindroth E, L'Huillier A and Dahlström J M 2014 Measurements of relative photoemission time delays in noble gas atoms *J. Phys. B* **47**(24), 245602

Itatani J, Quéré F, Yudin G L, Ivanov M Y, Krausz F and Corkum P B 2002 Attosecond streak camera *Phys. Rev. Lett.* **88**, 173903

Ivanov I A 2011 Time delay in strong-field photoionization of a hydrogen atom *Phys. Rev. A* **83**(2), 023421

Ivanov I A and Kheifets A S 2013 Time delay in atomic photoionization with circularly polarized light *Phys. Rev. A* **87**, 033407

Keller U 2014 *in* 'Frontiers of Intense Laser Physics' Kavli Institute for Theoretical Physics chapter Attosecond ionization dynamics

Klünder *et al* K 2011 Probing single-photon ionization on the attosecond time scale *Phys. Rev. Lett.* **106**(14), 143002

Lee H C, Jheng S D and Jiang T F 2012 Theory of infrared-dressed atomic photoionization by extremely ultraviolet attosecond pulse trains *J. Opt. Soc. Am. B* **29**(3), 286–293

Muller H 2002 Reconstruction of attosecond harmonic beating by interference of two-photon transitions *Applied Physics B: Lasers and Optics* **74**, s17–s21. 10.1007/s00340-002-0894-8

Nurhuda M and Faisal F H M 1999 Numerical solution of time-dependent Schrödinger equation for multiphoton processes: A matrix iterative method *Phys. Rev. A* **60**(4), 3125–3133

Palatchi C, Dahlström J M, Kheifets A S, Ivanov I A, Canaday D M, Agostini P and DiMauro L F 2014 Atomic delay in helium, neon, argon and krypton *J. Phys. B* **47**(24), 245003

Paul P M, Toma E S, Breger P, Mullot G, Aug F, Balcou P, Muller H G and Agostini P 2001 Observation of a train of attosecond pulses from high harmonic generation *Science* **292**(5522), 1689–1692

Pazourek R, Nagele S and Burgdorfer J 2013 Time-resolved photoemission on the attosecond scale: opportunities and challenges *Faraday Discuss.* **163**, 353–376

Sarsa A, Gálvez F J and Buendia E 2004 Parameterized optimized effective potential for the ground state of the atoms He through Xe *Atomic Data and Nuclear Data Tables* **88**(1), 163 – 202

Schoun S B, Chirla R, Wheeler J, Roedig C, Agostini P, DiMauro L F, Schafer K J and Gaarde M B 2014 Attosecond pulse shaping around a Cooper minimum *Phys. Rev. Lett.* **112**, 153001

Toma E S and Muller H G 2002 Calculation of matrix elements for mixed extreme-ultravioletinfrared two-photon above-threshold ionization of argon *Journal of Physics B: Atomic, Molecular and Optical Physics* **35**(16), 3435

Wätzel J, Moskalenko A, Pavlyukh Y and Berakdar J 2014 Angle-resolved time delay in photoemission *ArXiv e-prints* p. 1407.6613